AFRL-RD-PS
TP-2010-1027

THE AGGREGATE BEHAVIOR OF BRANCH POINTS- A PROPOSAL FOR AN ATMOSPHERIC TURBULENCE LAYER SENSOR: POSTPRINT

Darryl J. Sanchez, et al.

Air Force Research Laboratory
3500 Aberdeen Ave SE
Kirtland AFB, NM 87117

01 July 2010

Technical Paper

AIR FORCE RESEARCH LABORATORY
Directed Energy Directorate
3550 Aberdeen Ave SE
AIR FORCE MATERIEL COMMAND
KIRTLAND AIR FORCE BASE, NM 87117-5776

REPORT DOCUMENTATION PAGE

Form Approved
OMB No. 0704-0188

1. REPORT DATE *(DD-MM-YYYY)*	2. REPORT TYPE	3. DATES COVERED *(From - To)*
01-07-2010	Technical Paper	Oct 1, 2009- Jun 1, 2010

4. TITLE AND SUBTITLE
The Aggregate Behavior of Branch Points- A Proposal for an Atmospheric Turbulence Layer Sensor: Postprint

5a. CONTRACT NUMBER
In House DF702204

5b. GRANT NUMBER

5c. PROGRAM ELEMENT NUMBER

6. AUTHOR(S)
Darryl J. Sanchez, *Denis W. Oesch, Carolyn M. Tewksbury-Christle, Patrick R. Kelly

5d. PROJECT NUMBER

5e. TASK NUMBER

5f. WORK UNIT NUMBER

7. PERFORMING ORGANIZATION NAME(S) AND ADDRESS(ES)

Air Force Research Laboratory
3550 Aberdeen Ave SE
Kirtland AFB, NM 87117

*Science Applications International
2109 Airpark Road Southeast
Albuquerque, NM 87106-3236

8. PERFORMING ORGANIZATION REPORT NUMBER

9. SPONSORING / MONITORING AGENCY NAME(S) AND ADDRESS(ES)

Air Force Research Laboratory
3550 Aberdeen Ave
Kirtland AFB, NM 87117

10. SPONSOR/MONITOR'S ACRONYM(S)
AFRL/RDS

11. SPONSOR/MONITOR'S REPORT NUMBER(S)
AFRL-RD-PS-TP-2010-1027

12. DISTRIBUTION / AVAILABILITY STATEMENT

Approved for Public Release

13. SUPPLEMENTARY NOTES
Accepted for publication in the SPIE annual conference; August 4, 2010; San Diego, CA. 377ABW-2010-1145, July 1, 2010. "GOVERNMENT PURPOSE RIGHTS"

14. ABSTRACT

We propose a sensor that measures the number, strength, altitude and velocity of atmospheric turbulence layers, Recent research has shown that pupil plane branch points contain four independent and measureable parameters and that these four parameters can be used to estimate four independent turbulence layer parameters-number, strength, altitude and velocity—for each atmospheric turbulence layer. Here, we summarized previous results and then demonstrate how these results allow for construction of a turbulence layer sensor.

15. SUBJECT TERMS
Adaptive Optics, Branch Points, Atmospheric Turbulence

16. SECURITY CLASSIFICATION OF:			17. LIMITATION OF ABSTRACT	18. NUMBER OF PAGES	19a. NAME OF RESPONSIBLE PERSON
a. REPORT	b. ABSTRACT	c. THIS PAGE	SAR	28	Patrick Kelly
Unclassified	Unclassified	Unclassified			19b. TELEPHONE NUMBER *(include area code)* 505-846-2094

Standard Form 298 (Rev. 8-98)
Prescribed by ANSI Std. 239.18

This page is intentionally left blank.

The Aggregate Behavior of Branch Points - A Proposal for an Atmospheric Turbulence Layer Sensor

Darryl J. Sanchez[a], Denis W. Oesch[b], Carolyn M. Tewksbury[a] and Patrick R. Kelly[a]
[a] Starfire Optical Range, AFRL/RDS, Kirtland AFB, Albuquerque, NM. 87117, USA
[b] Science Applications International Corporation, Albuquerque, New Mexico, USA

ABSTRACT

We propose a sensor that measures the number, strength, altitude and velocity of atmospheric turbulence layers. Recent research has shown that pupil plane branch points contain four independent and measureable parameters and that these four parameters can be used to estimate four independent turbulence layer parameters--number, strength, altitude and velocity--for each atmospheric turbulence layer. Here, we summarized previous results and then demonstrate how these results allow for construction of a turbulence layer sensor.

Keywords: adaptive optics, branch points, atmospheric turbulence

1. INTRODUCTION

Much of astronomy relies on images collected through atmospheric turbulence. Turbulence imprints a random spatially varying phase on the propagating wave, and this random phase is an error that degrades image performance. Adaptive optics is a long established means of compensating for this error.

Traditional adaptive optics compensates for the errors by assuming a phase only disturbance in the pupil of the telescope, i.e. a singe turbulence layer at the pupil. A deformable mirror is placed optically conjugate to the pupil, and when the wave is reflected by the deformable mirror, the figure of the mirror is added to the phase of the optical wave, thus inverting the atmospheric phase disturbance. The deformable mirror's figure is calculated by subdividing the telescope's pupil into a regular array of subapertures and measuring the wave within each subaperture using a wavefront sensor. The corrupted phase is reconstructed from these measurements and fed into a proportional-integral controller that calculates deformable mirror commands. This long standing paradigm has been recently improved by both increasing the number of deformable mirrors, multi-conjugate adaptive optics (MCAO) and an enhanced controller (Predictive Fourier Control[1]). MCAO improves compensation by assuming a "best-fit" two layered structure to the atmospheric turbulence[2] even when the atmosphere is broadly distributed. This common assumption is borne out experimentally.[3] Predictive Fourier Control[1] modifies the control law to account for a layered atmosphere with each layer having a dominant velocity for a few tens of seconds. Hence, measurement of the three dimensional atmospheric turbulence is of interest because a priori knowledge of the turbulence layers can be used to improve adaptive optic compensation.

Of particular interest to us is a peculiar interference effect; after the wave encounters turbulence, as it propagates further, it self-interferes. Periodically, this self-interference creates zeros in amplitude. These zeros are known as branch points.

Here, we propose a sensor that uses branch points to measure the atmospheric turbulence layers. Branch points, in any classic adaptive optics sytstem, in particular one that uses a least mean square reconstructor only lead to degradation in adaptive optic system performance[4] and are regarded strictly as noise. In our previous work, we have shown that branch points contain a great deal of information about the turbulence that created them. In particular, we demonstrated that the ensemble of pupil-plane branch points carry four independent parameters.[5-9] These four independent parameters can be used to estimate four independent atmospheric turbulence layer parameters--number, strength, altitude and velocity.[8]

In this work, we describe a sensor that estimates those four parameters, describing how it can be built and implemented at an observatory. Specifically, we present the combined package of hardware and software necessary to build the sensor. We begin by first formulating the problem in Section 2 and and enumerating the parameters of importance for adaptive optics in Section 3. In Section 4, we address a seemingly major stumbling

block to successful implementation of this sensor. Then, in Section 5, we present our previous results; this is the foundation upon which this type of sesnor can be built. Section 6 presents the turbulence layer sensor, folowing which Section 7 discusses how this device was implemented in our laboratory. Finally, Section 8 summarizes the work. In these presentations, we demonstrate that branch points, which heretofore has been regarded strictly as noise in adaptive optics systems, can be used to estimate useful information on the turbulence layers.

2. THE ZEROS OF AN ANALYTIC FIELD

Assume that there is a monochromatic point source beyond the atmosphere and that a wave from this source propagates through the atmosphere. Atmospheric turbulence adds random optical path length to the propagating wave, and these path length differences appear as random phase fluctuations. As the wave propagates, the phase fluctuations cause the wave to self-interfere as it propagates. This self interference leads to amplitude fluctuations. Under the right conditions, this self-interference is strong enough to produce zeros in amplitude. These zeros in amplitude are known to appear when the log amplitude variance—called the Rytov parameter—of the propagating wave exceeds 0.1. Throughout the paper, the two terms 'zeros of the field' and 'branch points' will be used interchangably.

The field's zero in amplitude is both accompanied by an equivalent non-localized 2π circulation in phase, and also each zero is uniquely associated with either a positive or negative polarity. That is, in the absence of noise, when the phase, $\phi(x,y)$, is integrated about a closed path about a single branch point, the resultant is always $\pm 2\pi$,[4,10] i.e.

$$\int_{\Omega} dl\ \phi(x,y) = \pm 2\pi \tag{1}$$

where $\int_{\Omega} \cdot\ dl$ is a line integral along the closed curve Ω which encircles a single branch point. Note that the sign of the Equation 1 is uniquely associated with either ± 1. For discussional clarity, we call $sign\left(\int_{\Omega} dl\ \phi(x,y)\right)$ the polarity of the zero.

Properties of the zeros of the field are the foundation for creating a turbulence layer sensor.

Finding the Zeros

Finding the zeros of the field is of utmost importance. In the pristine world of theory, this is trivially done by finding the minima in the magnitude of the field. However, in the real-world, sensors have finite pixel size, and with probability one, this precludes using zeros to find branch points. In the real-world, in addition to having finite size pixels, they are also intrinsically noisy. In this case, it has been found that branch points are best found using Equation 1.[10,11]

Creation Pairs

It has been previously shown[9] that zeros appear in pairs of opposite polarity and that these pairs separate as they propagate. In addition to the density of branch points, intra-creation-pair separation is key to the design of a turbulence layer sensor.

3. PARAMETERS OF IMPORTANCE FOR ADAPTIVE OPTICS – WHAT A TULS MUST MEASURE

Atmospheric Turbulence and its Moments

Atmospheric turbulence causes phase disturbances. It has been found that the phase disturbances are best described by a structure function with an $\frac{11}{3}$ power law in its power spectrum; this is known as a Kolmogorov spectrum.[12] Assuming a Kolmogorov spectrum and using the Rytov approximation, two common approximation used in adaptive optics, it has been shown[12,13] that four moments of the atmospheric structure function, for the most part, determine adaptive optic performance. These are the zeroth altitude moment, the $\frac{5}{6}^{th}$ altitude

moment, the $\frac{5}{3}^{\text{th}}$ altitude moment, and the $\frac{5}{3}^{\text{th}}$ velocity moment. The functional forms of these moments for a plane wave are

$$\sigma_\chi^2 = 0.291 k_0^{7/6} \int_0^L C_n^2(h(z)) z^{5/6}\, dz \qquad \text{(Rytov parameter)} \qquad (2)$$

$$r_0 = \left(0.423 k_0^2 \int_0^L C_n^2(h(z))\, dz \right)^{-3/5} \qquad \text{(Fried's parameter)} \qquad (3)$$

$$\theta_0 = 2.91 k_0^2 \int_0^L C_n^2(h(z)) z^{5/3}\, dz \qquad \text{(the isoplanatic patch)} \qquad (4)$$

$$f_G = 0.254 k_0^{6/5} \left(\int_0^L C_n^2(h(z)) v^{5/3}(z) dz \right)^{3/5} \qquad \text{(Greenwood frequency)} \qquad (5)$$

with k_0 the wave number, L either the distance to the guide star or the top of the atmosphere. z the distance from the pupil to that point, $h(z)$ the altitude at distance z, and assuming a single-pole servo filter.

In the approximation of MCAO, turbulence is layered. Hence, the structure function is layered. Making the same assumption here, we assume that there are N_{turb} turbulence layers and these layers are at altitudes $h_1 < h_2 < \cdots < h_N$. The structure function is then given by

$$C_n^2(h) = C_n^2(h(z))\delta(h - h_1) + C_n^2(h(z))\delta(h - h_2) + \cdots + C_n^2(h(z))\delta(h - h_N). \qquad (6)$$

The Parameters of Interest in Adaptive Optics — r_0, σ_χ^2, θ_0 and f_G
A turbulence layer sensor must estimate the four parameters upon which r_0, σ_χ^2, θ_0 and f_G depend. These are the number of turbulence layers, and for each layer, its velocity, strength, and altitude.

4. CREATING BRANCH POINTS ON-DEMAND

One potential problem to practical implementation of a TuL Sensor is that for most observatories, no branch points exist in the optical field. For an observatory at an altitude of $3Km$ or greater, observing near zenith at wavelength of $1\mu m$, and using the Huffnagel-Valley atmospheric model, $\sigma_\chi^2 \ll 0.1$. This section demonstrates that this is not a problem because branch points can be produced on demand.

4.1 Branch Points, On-demand

In principle, all that is required to create branch points is to increase the propagation distance. To wit, suppose the actual Rytov parmater is near zero, but the required Rytov parameter is $\mathcal{R} > 0$. Since σ_χ^2 is monotonically increasing with z, then there exists Δz such that

$$\mathcal{R} = 0.291 k_0^{7/6} \int_0^L C_n^2(z)(z + \Delta z)^{5/6}\, dz$$

In the layered case, the h_i are fixed yielding

$$\mathcal{R} = 0.291 k_0^{7/6} \left(C_n^2(h)\delta(h - h_1)(h + \Delta z)^{5/6} + C_n^2(h)\delta(h - h_2)(h + \Delta z)^{5/6} \ldots \right.$$
$$\left. + C_n^2(h)\delta(h - h_N)(h + \Delta z)^{5/6} \right) \qquad (7)$$

the desired result.

4.2 Optically Increasing Propagation Distance

Unfortunately, Δz may be kilometers, so direct implementation on an optical bench is problematic. However, as is well known, propagating waves of the same Fresnel number are diffractively the same. The Fresnel number of an optical wave is given by

$$\mathcal{F} = \frac{(D/2)^2}{\lambda z} \tag{8}$$

with D the pupil diameter and λ the wavelength of the wave.

For two beams of different sizes, $D_{output} \neq D_{input}$, two beams are equivalent as long as z_{output} and z_{input} are adjusted such that

$$\mathcal{F} = \frac{(D_{output}/2)^2}{\lambda z_{output}} = \frac{(D_{input}/2)^2}{\lambda z_{input}}. \tag{9}$$

This fact is used by the optical community in every adaptive-optic optical design. For instance, consider a telescope; as the wave passes through a telescope, it is magnified by the telescope. Let D_{output} be the diameter of the input aperature and $D_{input} = MD_{output}$ be the diameter of the beam in the coudé room. If Δz_{opt} is required to obtain $\mathcal{F}$ and Δz_{input} is the maximum distance available in the coudé room, then choose M such that

$$\Delta z_{input} = M^2 \Delta z_{output} \tag{10}$$

Since M is selectable via the optical design, Δz_{output} of tens of kilometers can be equivalent to Δz_{input} of meters.

Note, since the altitude of turbulence layers is arbitrary, this technique varies the propagation distance, and hence the Rytov parameter at will, and this allows us to create branch points at will.

5. PREVIOUS RESULTS – MEASURING THE PARAMETERS OF INTEREST

In previous work, we have shown that the branch points of the field contain a rich amount of information. In the foundational work of this research thread,[9] it was shown that branch points are created in pairs of opposite polarity infinitesimally close together. Based on causality, it was speculated that branch points drift apart as they propagate, that the separation within creation pairs yields the distance to the turbulence layer that created this creation pair, and that the creation pairs have the velocity of the turbulence layer that created them. This is shown graphically in Figure 1. Later work expanded on this initial result greatly; this section reviews that work.

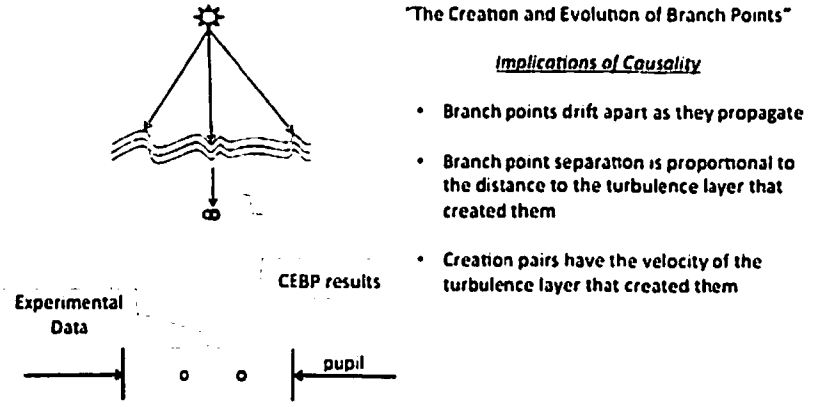

Figure 1. *A graphical view of the results of the foundational work for this research thread.*

The Polarity Sensor

In our previous work, a thought experiment sensor was assumed that measures an optical wave at time t_k and

returns a sensor frame (array) of data that contains ± 1 at the branch point locations and zeros elsewhere. Call this the polarity array and denote it $p(x, y, t)$. All the information needed for a turbulence layer sensor can be extracted from $p(x, y, t)$. This section enumerates the four independent parameters that are contained within $p(x, y, t)$.

5.1 The Velocity Distribution

The velocity distribution is created from the set of all possible velocities in $p(x, y, t_k)$. The set of all possible velocities is the set of all calculated velocities for all permutations of branch point velocities going forward in time for branch points of similar polarity.[5] Then create a function, $D(v)$, that takes the elements of the set of all possible velocities as input and returns the number of times each velocity occurs; $D(v)$ is the velocity distribution for this particular velocity set.

From $D(v)$, two parameters can be extracted, the number of velocity classes and the mean velocity of each class.

5.2 The Velocities Classes in $p(x, y, t)$

Branch points caused by the same atmospheric turbulence layer create self-correlating peaks in $D(v)$.[5] In the ideal case, these self-correlating peaks appear as delta functions in $D(v)$. Specifically, say there is a single turbulence layer with N_{BP} branch points, $D(v)$ will contain N_{BP} delta functions. Further, assume that each branch point is measured B_p times; in this case, the delta functions will have a coefficient with amplitude $\Gamma(B_p)$. The velocity distribution then contains this term:

$$\sum_{j=1}^{N_v} \Gamma(B_j)\delta(v - v_j). \tag{11}$$

where v_j is the location that the self-correlating peak occurs.

Each of these delta functions is a velocity class of the zeros of the field. In real-world data (see Section 7), due to noise and cross-terms in the distribution, these delta functions appear as large amplitude, sharply spiked peaks.

5.3 The Number of Velocities Classes and the Velocity of each Class

The Velocity

The velocities of the zeroes of the field are the locations of the delta functions in $D(v)$. In theoretical formulations, the velocities are the v_j found in the delta functions and can be read off directly from $\sum_{j=1}^{N_v} \Gamma(B_j)\delta(v - v_j)$. In real-world data, the velocities have to be estimated from the measured velocity distribution. This is done using

$$\{V_i\} = \{loc(max_{\text{loc}}(D^{meas}(v_x)))\} / \{0\} \tag{12}$$

where the $\{V_i\}$ are the velocities of each velocity class, $max_{\text{loc}}(\cdot)$ returns local maxima, $loc(max(\cdot))$ is the velocity at which those maxima occur, and $/\{0\}$ eliminates the zero due to the fixed pattern noise.

The Number

In theoretical formulations, the number of velocity classes is obtained by counting the number of delta functions in $D(v)$. In real-word data, the number of velocity classes is given by

$$N_{v.c.} = \dim(\{V_i\}) \tag{13}$$

where $N_{v.c.}$ is the number of velocity classes and $\dim(\cdot)$ is the number of delta functions in the velocity distribution (the dimension of the set $\{V_i\}$).

The Importance of Velocity Classes

Finding the velocity classes is of fundamental importance to creation of the turbulence layer sensor. Velocity

classes not only give us the two parameters above, but just as importantly, they allow us to sort branch points into velocity classes. Sorting branch points into a velocity class allows us to measure both density and creation pair separation for that class.

A cartoon showing why separation into velocity classes is possible is presented in Figure 2. Laboratory data, in this case for velocity filtering, is shown in Figure 3.

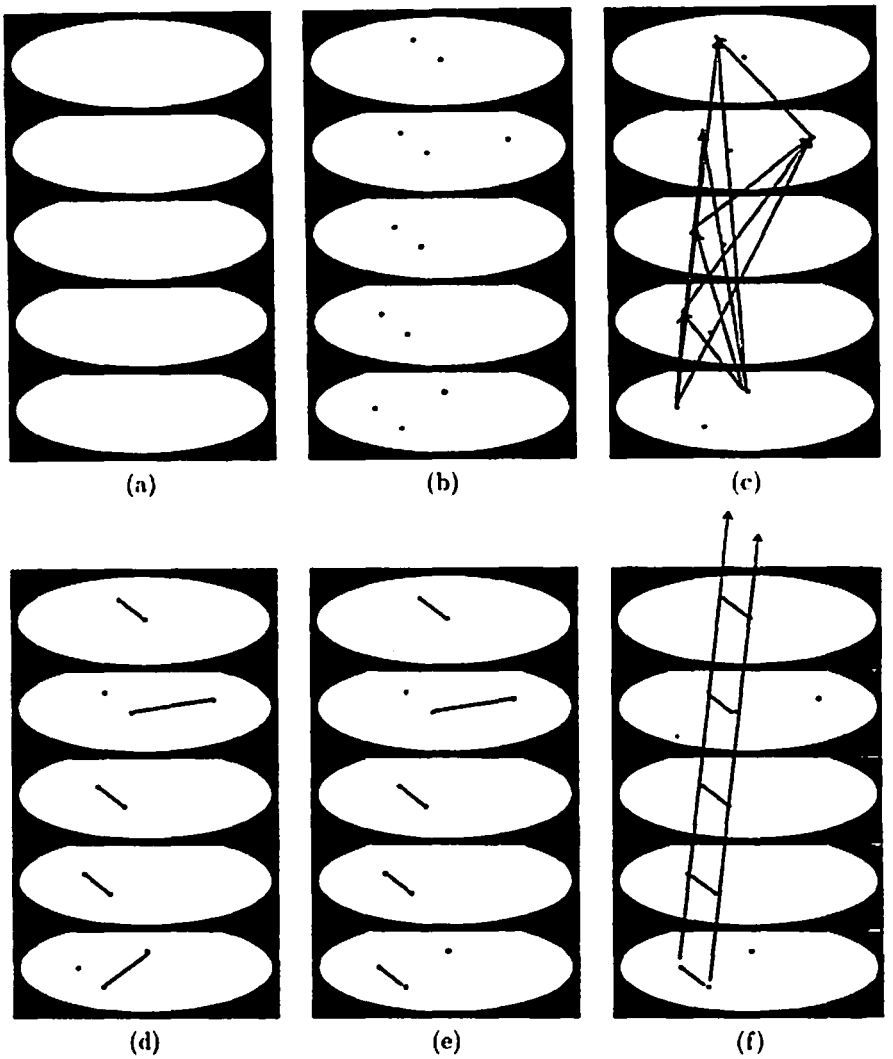

Figure 2. *Cartoon of the steps in the identification of persistent pupil plane branch point pairs. Red and green dots indicate the positive and negative circulations respectively. (a) The empty polarity array. (b) The polarity array with ±1's at the locations of positive and negative circulations respectively. (c) Diagram showing the estimated velocities from the positive branch point locations. (d) Blue lines indicate the initial pairings following frame by frame use of a walking algorithm. (e) Pairings following the use of piston shifting technique. (6) Overlay of measured velocity to incorporate 3rd dimension of WFS data.*

5.4 Creation Pair Separation (Δ)

Each branch point is placed in its velocity class. Then, for each velocity class, let Δ_i be the mean separation between creation pairs. It has been shown[8,14] that the inter-pair separation decreases in a well defined way with

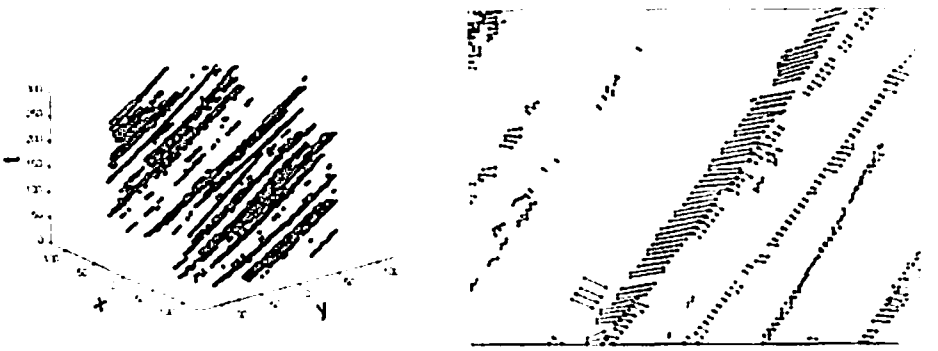

(a) (b)

Figure 3. *A polarity array shown in 3-D (left) and a blowup of the output of the pairing algorithm (right). This type of processing allows us to place branch points into velocity classes, of fundamental importance for finding Δ_i and δ_i.*

turbulence strength and propagation distance. For the the turbulence layers in our laboratory

$$\Delta_i \propto (C_{n,i}^2)^{-11/10} z_i^{-11/12}. \tag{14}$$

with z_i the propagation distance to turbulence layer i and $C_{n,i}^2$ the turbulence strength of layer i

5.5 Intra-creation Pair Separation (δ)

For each velocity class, let δ_i be the mean separation between the positive and negative branch points within a creation pair. It has been shown[8] that the intra-pair separation increases in a well defined way with propagation distance. For the turbulence layers in our laboratory, we have shown

$$\delta_i \propto \sqrt{z_i} \tag{15}$$

where z_i the propagation distance to turbulence layer i. The proportionality to $\sqrt{z_i}$ matches a much earlier observation by Tatarskii[15] and gives us great confidence in the veracity of these results. Our experimental work is on-going, but a finer estimate at the current time appears to be

$$\delta_i \propto (z_i - z_{0,i})^{1/2} \tag{16}$$

with z_i as before and $z_{0,i}$ the distance to the onset of branch points for turbulence layer i.

6. THE TURBULENCE LAYER SENSOR

Conceptually, this sensor is simple. It takes as input an optical wave in the pupil plane of a telescope and returns as output the number, velocity, altitude and strength of the atmospheric turbulence layers. Since four independent turbulence layer parameters are desired to be found, four independent parameters, related to the output parameters, must be found. (Note that the four parameters contain, in reality, $4N_{v.c.} + 1$ variables.) Specifically,

Turbulence Parameters				*Pupil-plane Parameters*
# of turbulence layers	N_{turb}	$\Longleftrightarrow$	$N_{v.c.}$	# of velocity classes
velocity of the turbulence layers	V_i		v_i	mean of each velocity class
altitude of the turbulence layers	h_i		Δ_i	branch point density
strength of the turbulence layers	$C_{n,i}$		δ_i	intra-pair separation

Whence the four pupil plance parameters was described in Section 5. The purpose of this section is to describe the device that measures the four pupil plance parameters, and how that device converts those parameters into useful information. This includes a description of how the sensor would be operationally used, the optics necessary, the algorithms that convert the raw wavefront sensor data into the polarity array, the algorithms that translate the polarity into meaningful output data, and TuLS at your observatory.

6.1 Cartoon and Description of The Sensor's Components

The turbulence layer sensor can be broken into three major components, the optics, the polarity sensor, and the processing algorithms. These are shown pictorially in Figure 4. The optics capture the input light, add propagation distance as required, and relay it to the polarity sensor. The polarity sensor is comprised of a wavefront sensor with additional processing; its output is the polarity array at each propagation distance. The polarity arrays are passed to the processing system where the turbulence layer parameters are calculated.

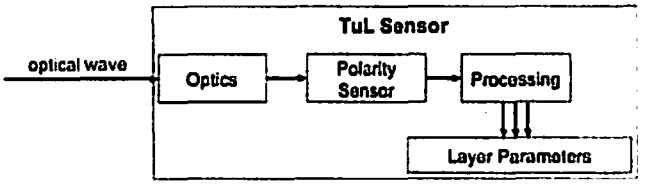

Figure 4. *A four block diagram of the TuL sensor (shown in gray).*

The sensor takes time resolved measurements of the field at different propagation distances. The purpose of the measurements is to take enough data to sort branch points into velocity classes and measure Δ_i and δ_i for each velocity class. To do this, firstly, the sensor creates branch points. At the cartoon level, Figure 5 shows pictorially how this is done. A point source is shown above the atmosphere, propagating through it to the pupil of the telescope. The TuLS is shown in gray. It takes the input wave and increases the propagation distance until branch points form; the branch points are shown as blue and green circles. The propagation distance is then repeatedly increased (shown as the z_i) with time-resolved measurements of the field taken at each propagation distance.

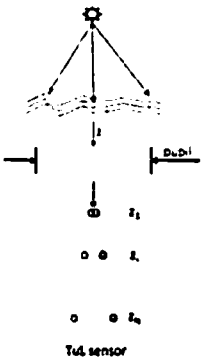

Figure 5. *A pictorial view of how the turbulence layer sensor varies its parameter space; it repeated increases propagation distance, taking time-resoved measurements of the field at each distance. The TuLS is shown as the gray box beneath the telescope's pupil.*

6.2 The Optics

Other than simple relays, the optics must accomplish two tasks, first, it must cookie-cut the pupil to a proper dimension (see below) and second, it must create additional propagation as required by the algorithms. To do this, the optics first capture the input beam passed by the primary optical beam train. For simplicity, we will assume that a pupil is relayed to the TuLS input aperture. (This is not really required for the TuLS to work; however, if this is not the case, additional optics are required, trivial to implement but not addressed here.) A piece of the input aperture is selected to be interrogated. This piece of the pupil is relayed to an optical trombone which adds additional propagation as required by the algorithms. It is then relayed to a wavefront sensor which measures the field and outputs the sampled wavefront at known time intervals sufficiently small in order to time resolve

the field. This is shown pictorially in Figure 6. The remainder of the system is processing to be discussed in Section 6.4.

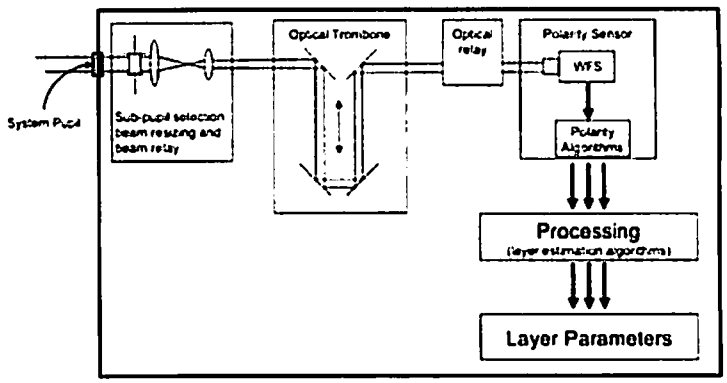

Figure 6. *A cartoon of TuLS showing additional detail on the type of optics required.*

Discussion Concerning The Pupil

The TuLS takes as input a pupil, that is, a telescope pupil is relayed to the input aperture of the TuLS. For large telescopes, only a piece of the pupil is necessary. For instance, in our laboratory, we mock up a $1.5m$ pupil. So, for large telescopes, the first thing TuLS does is limit the aperture to approximately $1.0m$.

The size of the aperture necessary is determined by the wind speed. The slower the wind speed, the smaller the interrogated piece of the aperture must be. This is because the wind speed and aperture size determine the number of times each branch point pair is measured prior to exiting the pupil.[16]

Discussion of The Trombone

The trombone is the optical component that adds additional propagation distance. The distance to be added depends on the altitude and strength of the turbulence layers. Since the structure function is a function of altitude, given by an atmospheric model, for instance the Huffnagel-Valley model, the strength dependence can be obtained once the altitude is known. In output space, for our laboratory, all additional propagation was less than $20Km$ and for most runs, it was less then $12Km$. Given these distances, once an input beam size is optically fixed, the length of the trombone is determined by Equation 9. For our benchtop implementation, the trombone moves less than $140cm$.

The presicion to which the on-bench trombone must be moved is a function of Equations 9 and 10. For our benchtop implementation, trombone movement of $1mm$ is sufficient.

Discussion of The Polarity Sensor

The polarity sensor is composed a wavefront sensor with additional processing that calculates the polarity array. The wavefront sensor can be any standard design, for instance, a Shack-Hartmann or self-referencing interferometer. It can operate in any band from the visible to the near IR, but operation in the visible will decrease the trombone length. The number of wavefront sensor subapertures depends on the pupil size; for our laboratory data, a sensor with 200x200 pixels was used on an output aperture size of $1.5m$. The frame rate of the camera is determined by the wind velocity; take enough samples per the wind's corellation time to resolve the motion. Note, wavefront sensors currently installed at astronomical observatories will have difficulty detecting the branch points since the supaperture size is so large.

6.3 The Parameter Sets Required to Estimate the Turbulence Parameters

The TuLS requires time resolved open loop samples of the field. The number of samples depends on the depends on the wind speed, the size of the pupil mapped to the WFS, as well as, noise. For our laboratory data, 200

uncorrelated measurements at each propagation distance was sufficient. Data measured at ten propagation distances after the onset of branch points is sufficient to get good estimates.

6.4 Processing

There are six indpendent algorithms that must be run to calculate the four pupil plane parameters. These will be discussed in turn.

Assume that the wavefront sensor has measured a sufficient number of frames of data at each propagation distance. Then, for each propagation distance, the following algorithms are run in the order given. References to the previous paper that describes the results are annotated. The first algorithm finds the location and polarity of the branch points, loads the polarity array, and calculates the overall branch point density (see[3,6,10]). The second algorithm calculates the velocity distribution (see[5]). The third algorithm establishes an initial branch point pairing using in-frame branch cuts (see[7]). The forth algorithm identifies the creation pairs using the results of the third algorithm and velocity filtering (see[7]). The fifth algorithm finds the velocity classes of the polarity array (see[16]). The sixth algorithm equates a velocity with each unique subset of $p(x, y, t)$ and the creation pairs are assigned to a unique subset (see[7,8]). Once these six algorithms have completed, we have in-hand the polarity array, and the velocity distribution for this polarity array. As described in Section 5, from these, four independent pupil plane parameters can be calculated. These are

1. the number of velocity classes contained in the velocity distribution,
2. the mean velocity of each velocity class,
3. the creation pair separation for each velocity class, and
4. the intra-pair separation for each velocity class.

As is stated in,[8] these four parameters are all that is required to calculate four turbulence layer parameters.

Turbulence Layer Estimation — Number

The number of turbulence layers, N_{turb} is equal to the number of velocity classes, $N_{v.c.}$.

$$N_{turb} = N_{v.c.} \tag{17}$$

Turbulence Layer Estimation — Velocity

The velocity of each turbulence layer, V_i, is the scaled velocity of each velocity class in $p(x, y, t)$.

$$V_i = C_v \, v_i \tag{18}$$

where i denotes the i^{th} layer, v_i is the measured speed in pixels/frame, V_i is the turbulence velocity in meters/second and C_v is a constant particular to each experimental setup. For our testbed, $C_v = 1000\left(\frac{1.5}{240}\right) = 6.25$.

Turbulence Layer Estimation — Altitude and Strength

The strength and altitude of each turbulence layer is found by inverting the Δ and δ curves for each velocity class.

For data taken in our laboratory,[8] the turbulence strength is given as

$$C_{n,i}^2 = c \, \delta_i^{11/3} \, \Delta_i^2 \tag{19}$$

where c is a constant, and the altitude of the layer is

$$z_i = 1 + d \, z_{0,i} \, \delta_i^2 \left(C_{n,i}^2\right)^{6/5} \tag{20}$$

where d is a constant and z_0 the distance to the onset of branch point formation. We make no claim, as yet, that these results are definitive, merely that they are suggestive that well-defined curves exists in nature, and these curves can be inverted.

6.5 TuLS at your Observatory

While the previous sections outlined theoretical considerations for the TuLS, this section covers practical issues.

Where in the system would it (could it) go?
The TuLS requires open loop data. Hence, a logical place would be prior to the steering mirror (we assume that standard adaptive optics system: the beam encounters a steering mirror followed by the deformable mirror followed by the wavefront sensor). Also, this device would best be permanently installed on the optical system; this is not a requirement, but would reduce down time due to realignment at each data collection.

How does it get light (pick off considerations)?
A slide-based pickoff mirror could be placed in the optical system and inserted for TuLS data collection; a dichroic pickoff would also be useable here. However, it could also be placed after the deformable mirror, as long as, the system is running open loop while TuLS is collecting data.

Isolation requirements
A TuLS sensor would have the same requirements as a wavefront sensor, i.e. a vibration stabilized part of the beam train. Temperature fluctuations would not be a consideration outside of this, that is, changes to trombone length would not affect successful operation.

How big is it?
A design could easily fit TuLS within a $2m$x$2m$ part of the optical bench. This could be reduced if bench space is at a preimium.

When to use it?
The device would be used often enough to determine bulk wind velocity. This would be a few times per night in the general vicinity of the science object. Also, the data collection would take no more than a few minutes. At present, the processing takes a few hours using off-the-shelf PCs; investment in dedicated processors could shorten this to minutes.

The Sensor in Operation – How do you use it?
To be used, first a bright unresolved star must be found in the general vicinity of the science object. Insert the flip mirror, redirecting the light to TuLS. Do a quick scan for turbulence producing layers, finding the general altitudes of the strong layers. Set TuLS at the altitude (Δz_{input}) of the lowest turbulence layer, then take data in increasing $500m$ increments from that point. Finally, run the analysis scripts. The total time to do this will be determined by the brightness of the source and the speed of the turbulence, but it should be no more than a few minutes.

7. IMPLEMENTATION OF TULS IN ASALT AND RESULTS FOR THAT IMPLEMENTATION

A version of the TuL sensor was implemented in the ASALT laboratory. This section presents how this was done along with results from that implementation.

7.1 The Optics and Optical Hardware

Instrumentation
The data presented here is taken on a testbed equipped with a well calibrated atmospheric turbulence generator[17] consisting of two 6-inch disks, each etched with a Kolmogorov structure function. To this standard simulator, we added a variable length optical trombone. These are shown in Figure 7. There we see, in the lower left corner, the turbulence simulator, followed by the trombone's pickoff mirror, followed immediately by the trombone. The next, the standard components of an adaptive optics sytem are seen, the steering mirror, the deformable mirror

and the wavefront sensor. Due to our limited budget, the adaptive optic's wavefront sensor was used in lieu of a dedicated wavefront sensor; this is possible because our standard wavefront sensor is eight times oversampled.

A typical parameter set for a velocity measurement is shown in Table 1. For purposes here, only two items are of note. First, in column two the number of frames is 200, that is, only two hundred independent measurements are required for us to obtain estimate the turbulence. in real-world data, this would be tens of seconds since the branch points must cross wavefront sensor subapertures in order to be observed. Second, these tests have two turbulence layers. Also (obviously), for full turbulence layer estimation, variation in propagation distance would also have to be done.

		Turbulence Conditions					ATS Configuration	
Table Config.	Number of Frames	Turb. Strength C_n^2 ($m^{2/3}$)	Turb. Velocity (low, high) (m/s)	Turb. Altitude (low, high) (km)	in pupil r_0 (cm)	σ_χ^2	Position (low, high) (cm)	Velocity (low, high) (steps/frame)
1	200	$2.013 \cdot 10^{-15}$	(3.3, −39.6)	(1.8, 4.8)	6.91	0.19	(99.0, 55.5)	(1, −3)
2	200	$1.579 \cdot 10^{-15}$	(4.6, -0.3)	(0.0, 21.6)	8.12	0.29	(102.5, 47.5)	(1, -3)
3	200	$2.414 \cdot 10^{-15}$	(3.3, -0.3)	(1.8, 21.6)	6.25	0.47	(99.0, 47.5)	(1, -3)

Table 1. *Turbulence parameters used to demonstrate both that our method is invariant with respect to turbulence strength and also that the assumption of branch point persistence has experimental basis. Bold print is used to identify the branch point producing layers.*

7.2 Experimental Results

For the parameters in Table 1, data was collected and the polarity array calculated. Projections of the polarity arrays onto the $x-t$ plane are plotted in Figs. 8 plots (a), (c), and (e); branch point trajectories through the array are readily apparent. The velocity distributions, $D(v_x)$ are shown in Figs. 8 plots (b), (d), and (f). The peaks, characteristic of turbulence layers, are readily apparent.

Number and Velocity of Turbulence Layers

Focusing on the delta functions in the velocity distributions, we see that the number of turbulence layers is one, one and two, for Configurations 1, 2, and 3, respectively, just as was set in Table 1. Turning our attention to the location of the delta function, for Configuration 1, the single strong peak is centered at 0.5 *pixel/frame*, for Configuration 2, the single strong peak is centered at -1.5 *pixel/frame*, for Configuration 3, the two strong peaks are centered at 0.5, -1.5 *pixel/frame*, just as was set in Table 1.

Strength and Distance of the Turbulence Layers

Many other datasets have been taken; Table 2 tabularizes the parameter sets for one such data run. In these runs the turbulence was set at eleven strengths, and at each of these strengths the propagation of the layer to the measurement device was increased. Results for this representative data set showing the variation in propagation--necessary to estimate Δ and δ--are shown in Figure 9. Each filled circle represents a data point.

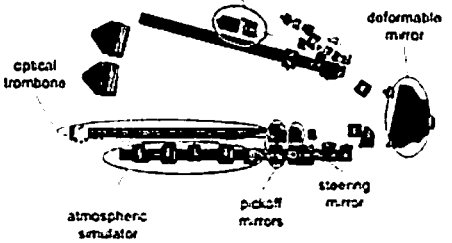

Figure 7. *The turbulence layer sensor implemented on our testbed. the opto-mechanical CAD drawing of the optical hardware as it appears on our bench.*

For these datasets and using the techniques already mentioned, the curves were inverted to yield Equation 19 for turbulence strength and Equation20 for turbulence altitude.

			ATS Configuration			Turbulence Conditions			
Ensemble Set #	Number of Realizations	Lens Set	Trombone Position (cm)	PW Position (low, high) (cm)	PW Step (low, high) (counts)	Propagation Range (km)	Turb. Velocity (low, high) (m/s)	r_0 (cm)	σ_χ^2
1	200	7	{0:5:50}	(106.3, *puck*)	(3, 0)	0.0-8.4	(11.75, 0)	16.6	0.00 – 0.15
2	200	7	{0:5:50}	(105.5, *puck*)	(3, 0)	1.5-9.8	(10.22, 0)	14.4	0.04 – 0.22
3	200	7	{0:5:50}	(104.5, *puck*)	(3, 0)	2.8-11.1	(8.79, 0)	12.4	0.10 – 0.32
4	200	7	{0:5:50}	(104.0, *puck*)	(3, 0)	3.3-11.7	(8.22, 0)	11.6	0.13 – 0.37
5	200	7	{0:5:50}	(103.5, *puck*)	(3, 0)	3.8-12.1	(7.71, 0)	10.9	0.16 – 0.42
6	200	7	{0:5:50}	(103.0, *puck*)	(3, 0)	4.2-12.6	(7.27, 0)	10.3	0.19 – 0.48
7	200	7	{0:5:50}	(102.5, *puck*)	(3, 0)	4.6-12.9	(6.87, 0)	9.7	0.23 – 0.54
8	200	7	{0:5:50}	(101.5, *puck*)	(3, 0)	5.2-13.5	(6.20, 0)	8.8	0.30 – 0.67
9	200	7	{0:5:50}	(101.0, *puck*)	(3, 0)	5.4-13.8	(5.91, 0)	8.3	0.34 – 0.73
10	200	7	{0:5:50}	(99.5, *puck*)	(3, 0)	6.1-14.4	(5.18, 0)	7.3	0.46 – 0.95
11	200	7	{0:5:50}	(98.0, *puck*)	(3, 0)	6.6-15.0	(4.61, 0)	6.5	0.60 – 1.19

Table 2. *Turbulence parameters used for measurement of branch point separation. For each Ensemble set, 200 frames of data was collected for each of 11 positions of the optical trombone, ranging in 5 cm increments from 0 to 50 cm. This corresponds to ranges of propagation distances and Rytov parameters for each Ensemble. The term 'puck' refers to the clear center portion of the phase screen. To be placed at 'puck' means the light was passing through the center of the screen and not contributing to the turbulence simulated by the ATS.*

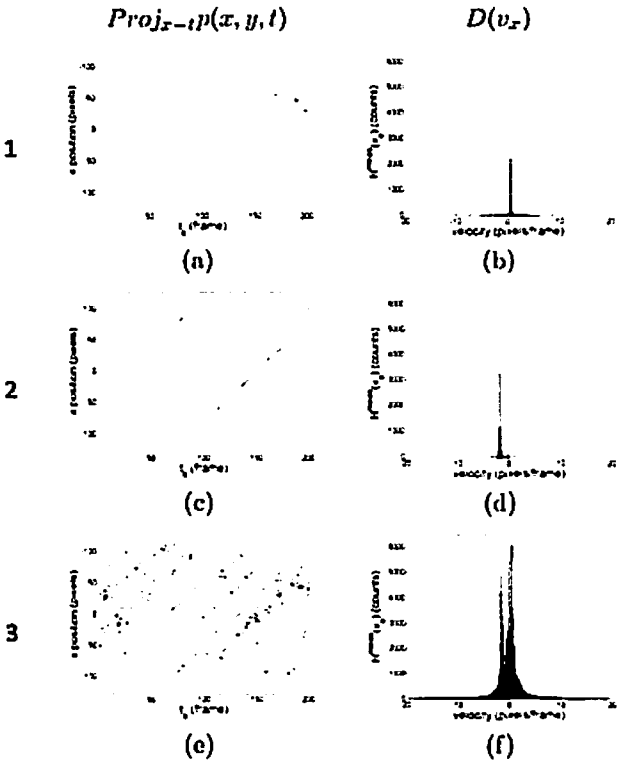

Figure 8. *Initial demonstration data for Table 1. Left column: x-t projections of $p(x,y,t)$. Right column: matching velocity distributions, $D(v_x)$. Top row: Table Configuration 1: r0 = 6.91, $\sigma_\lambda^2 = 0.19$. Middle row: Table Configuration 2: r0 = 8.12, $\sigma_\lambda^2 = 0.29$. Bottom row: Table Configuration 3: r0 = 6.25, $\sigma_\lambda^2 = 0.47$. In each case both phase wheels were spinning, $v_{bench} = (1,-3)$. In Config. 1 the branch points are associated with the low altitude phase wheel and the spike is at 0.5pixels/frame. In Config. 2 they are associated with the high altitude phase wheel and the spikes is at −1.5pixels/frame. In Configuration 3, branch points form from both layers and two non-zeros spikes are seen at −1.5 and 0.5pixels/frame respectively.*

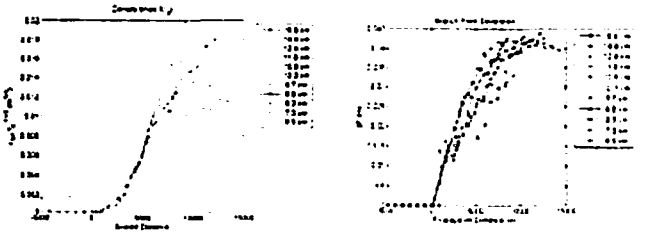

Figure 9. *Density is shown in plot (a), and separation in plot (b). Both are scaled and normalized properly.*

8. DISCUSSION AND SUMMARY

Here, we proposed a sensor that measures the number, strength, altitude and velocity of atmospheric turbulence layers. This is based on our previous work linked the zeros of the field to the turbulence layer that created them. Our other recent research has shown that the zeros of the optical wave contain four independent parameters that can be measured. These four independent parameters can be used to estimate four independent turbulence layer parameters--number, strength, altitude and velocity--for each atmospheric turbulence layer. Though branch points are not commonly present in the observing geometry typically used in astronomy, it is trivial to show that by artificially increasing the propagation distance using an optical trombone, branch points can be created on demand.

Here we presented the rationale for a sensor that creates branch points, measures four independent pupil plane parameters and estimates four atmospheric turbulence layer parameters. We also presented an implementation of this sensor in the ASALT laboratory. Within the assumptions of a layered atmosphere and Taylor flow, the proposal to for this sensor is well founded; however, more work is necessary and on-going. First, these results must be extended to study the effect of broadband light on the measurements. Secondly, the veracity of these results in the presence of a distributed atmosphere must be confirmed. Finally, these results have to be validated in field experiments; a plan to do so has been conceived, but a field device has not yet been built. This research is on-going and results will be presented as they become available; in particular, we invite you to our upcoming presentation at IEEE in Big Sky, Montana where we will present wave optic simulation of this same effect and our related work in controling a $mod(\lambda)$ device

REFERENCES

1. L. A. Poyneer, B. A. Macintosh, and J. P. Véran, "Fourier transform wavefront control with adaptive prediction of the atmosphere," *JOSA* **24**(9), pp. 2645–2660, 2007.
2. D. C. Johnston and B. M. Welsh, "Analysis of multiconjugate adaptive optics," *Applied Optics* **11**(1), pp. 394–408, 1994.
3. L. Poyneer, M. van Dam, and J. P. Véran, "Experimental verification of the frozen flow atmospheric turbulence assumption with use of astronomical adaptive optics telemtry," *JOSA* **26**(4), pp. 833–846, 2009.
4. D. L. Fried, "Branch point problem in adaptive optics," *Journal of the Optical Society of America* **15**, pp. 2759–2768, October 1998.
5. D. W. Oesch, D. J. Sanchez, P. R. Kelly, K. P. Vitayaudom, C. M. Tewksbury-Christle, J. Smith, and N. E. Glauvitz, "The Aggregate Behavior of Branch Points: An Overview of Research in the ASALT lab," in *2009 DEPS Annual Conference*, D. Herrick, ed., Directed Energy Professional Society, 2009. Published in briefing format only.
6. D. W. Oesch, D. J. Sanchez, C. M. Tewksbury-Christle, and P. R. Kelly, "The Aggregate Behavior of Branch Points - Branch Point Density as a Characteristic of an Atmospheric Turbulence Simulator," in *2009 SPIE Annual Conference*, R. Carerras, T. Rhoadharmer, and D. Dayton, eds., SPIE, 2009.
7. D. W. Oesch, D. J. Sanchez, C. M. Tewksbury-Christle, and P. R. Kelly, "The aggregate behavior of branch points - persistent pairs within atmospheric turbulence layers," in *2010 DEPS Annual Conference*, D. Herrick, ed., Directed Energy Professional Society, 2010.
8. D. W. Oesch, D. J. Sanchez, C. M. Tewksbury-Christle, and P. R. Kelly, "The aggregate behavior of branch points - altitude and strength of atmospheric turbulence layers," in *2010 SPIE Annual Conference*, T. Rhoadharmer, D. Dayton, and D. J. Sanchez, eds., SPIE, 2010. In preparation.
9. D. J. Sanchez, D. W. Oesch, C. M. Tewksbury-Christle, and P. R. Kelly, "The Aggregate Behavior of Branch Points - The Creation and Evolution of Branch Points," in *2009 SPIE Annual Conference*, R. Carerras, T. Rhoadharmer, and D. Dayton, eds., SPIE, 2009.
10. D. L. Fried, "Crypto branch points: a problem in phase unwrapping," Tech Note TN-190, David Fried, February 2005.
11. D. L. Fried, "Using the hidden phase formulation in wave front reconstruction," Tech Note TN-100, David Fried, August 1999.

12. R. J. Sasiela, *Electromagnetic Wave Propagation in Turbulence: Evaluation and Application of Mellin Transforms*, Bellingham, Wa. USA, 1 ed., 2007.
13. D. Washburn and R. R. Butts, "Does the detailed turbulence profile matter?." Completed while working for the Air Force Research Laboratory.
14. D. J. Sanchez, D. W. Oesch, C. M. Tewksbury-Christle, and P. R. Kelly, "Fitting error in deep turbulence for a flat subaperture segmented deformable mirror," in *2010 SPIE Annual Conference*, T. Rhoadharmer, D. Dayton, and D. J. Sanchez, eds., SPIE, 2010. In preparation.
15. V. I. Tatarskii, *The Effects Of Turbulent Atmosphere On Wave Propagation*, Israel Program for Scientific Translations Ltd., Jerusalem, 1971.
16. D. W. Oesch and D. J. Sanchez, "The aggregate behavior of branch points - measuring the number and velocity of atmospheric turbulence layers," In preparation. To be submitted to Optics Express.
17. S. V. Mantravadi, T. A. Rhoadarmer, and R. S. Glas, "Simple laboratory system for generating well-controlled atmospheric-like turbulence," in *Advanced Wavefront Control: Methods, Devices, and Applications II*, M. K. Giles, J. D. Gonglewshi, and R. A. Carerras, eds., *Presented at the Society of Photo-Optical Instrumentation Engineers (SPIE) Conference* **5553**, pp. 290–300, Oct 2004.

DISTRIBUTION LIST

DTIC/OCP
8725 John J. Kingman Rd, Suite 0944
Ft Belvoir, VA 22060-6218 1 cy

AFRL/RVIL
Kirtland AFB, NM 87117-5776 2 cy

Patrick Kelly
Official Record Copy
AFRL/RDSAE 1 cy